Electronic Supplementary Information

Small-Molecule Organic Ferroelectric Piezoelectric Voltage Coefficient Larger than Lead Zirconate Titanate and Polyvinylidene Difluoride

Han-Yue Zhang[a,] *

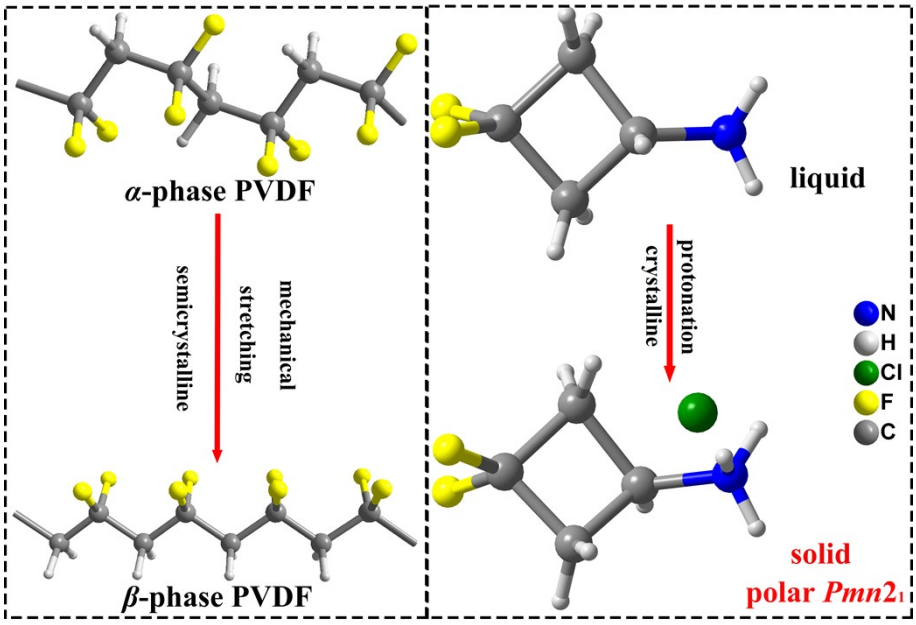

Scheme S1. Design strategy of (3,3-DFCBA)Cl. Comparison of the ways to obtain ferroelectric phase of the ferroelectric polymer PVDF and small-molecule ferroelectric (3,3-DFCBA)Cl.

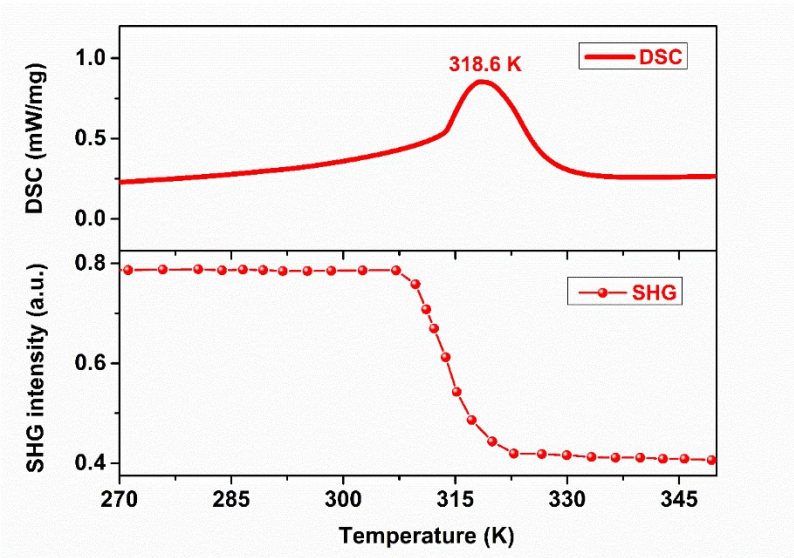

Fig. S1. DSC curve and temperature-dependent SHG intensity of (CBA)Cl in the heating run, showing phase transition at 318.6 K.

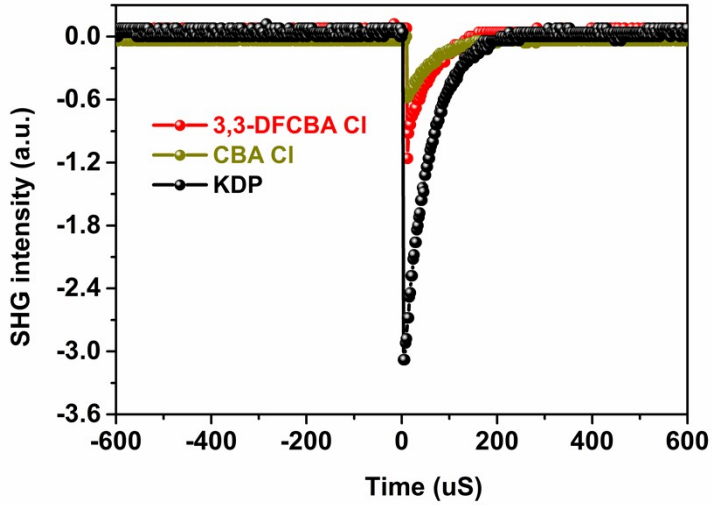

Fig. S2. SHG signals of (3,3-DFCBA)Cl, (CBA)Cl and KDP at room temperature.

Calculation of polarization of (3,3-DFCBA)Cl according to a point charge model

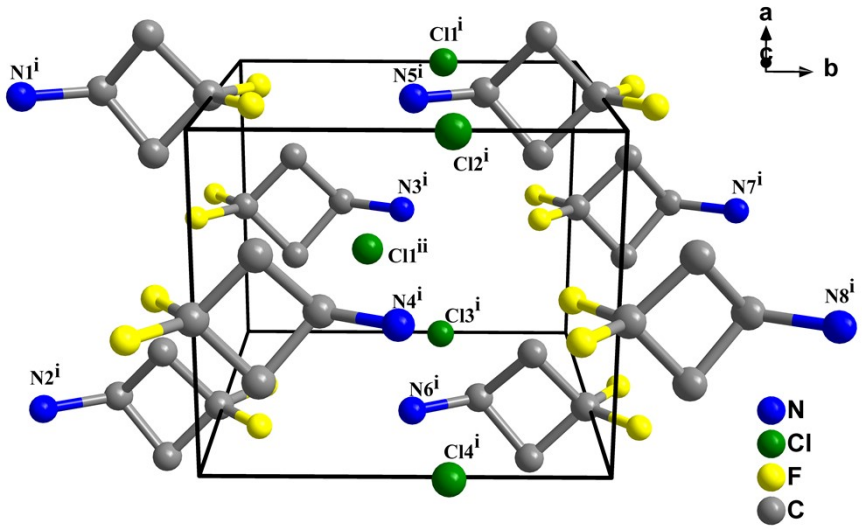

Fig. S3. Distribution of Cl and N atoms of (3,3-DFCBA)Cl in a unit cell.

According to the crystal structure data collected at 293 K, we select a unit cell and assume that the centers of the positive and negative charges of the (3,3-DFCBA)Cl are located on the N atoms and Cl atoms, respectively.

Atoms	Atom coordinate		Coordinate of charge center
N	$N1^{i}$ (1, -0.4832, 0.3944)	$N5^{i}$ (1, 0.5168, 0.3944)	(0.5, 0.5, 0.3944)
	$N2^{i}$ (0, -0.4832, 0.3944)	$N6^{i}$ (0, 0.5168, 0.3944)	
	$N3^{i}$ (0.5, 0.4832, 0.8944)	$N7^{i}$ (0.5, 1.4832, 0.8944)	
	$N4^{i}$ (0.5, 0.4832, -0.1056)	$N8^{i}$ (0.5, 1.4832, -0.1056)	
Cl	$Cl1^{i}$ (1, 0.6056, 0.9864)	$Cl3^{i}$ (0, 0.6056, 0.9864)	(0.5, 0.5, 0.4864)
	$Cl2^{i}$ (1, 0.6056, -0.0136)	$Cl4^{i}$ (0, 0.6056, -0.0136)	
	$Cl1^{ii}$ (0.5, 0.3944, 0.4864)		

$$P_s = \lim \frac{1}{V} \sum q_i r_i$$

$$= (q_{Cl} r_{Cl} + q_N r_N) / V$$

$$= [(-e \times 0.4864) + (e \times 0.3944)] \times 2 \times c/V$$

$$= [-0.092 \times 2 \times 1.6 \times 10^{-19} \times 7.6493 \times 10^{-10}\ C\ m] / (327.87 \times 10^{-30}\ m^3)$$

$$= -6.9 \times 10^{-2}\ C\ m^{-2}$$

$|P_s| = 6.9 \times 10^{-2}\ \mathrm{C\ m^{-2}} = 6.9\ \mu\mathrm{C\ cm^{-2}}$

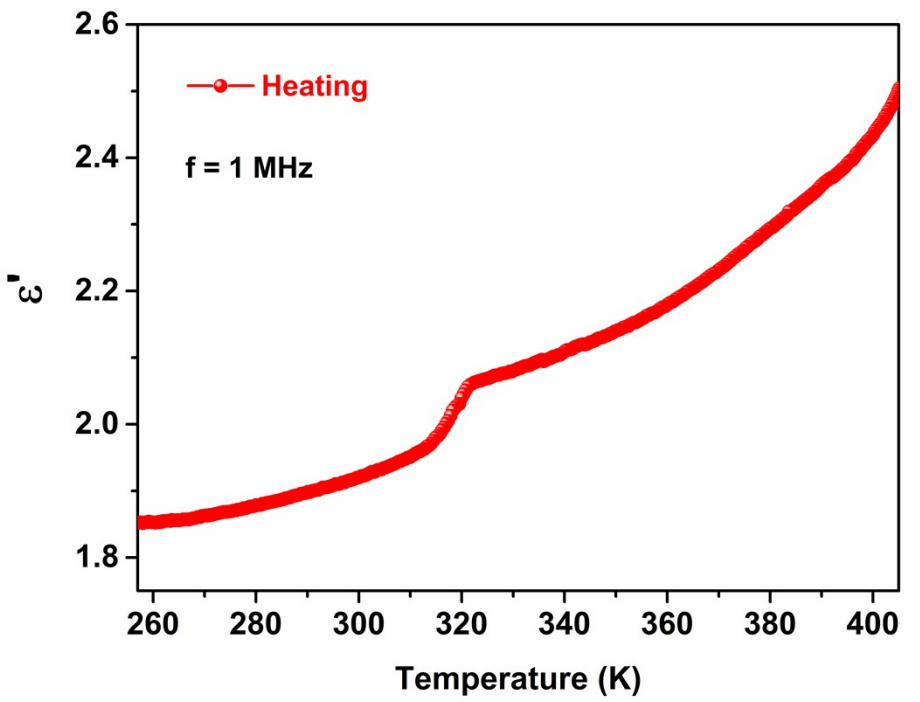

Fig. S4. The dependence of the real part ε' of (CBA)Cl at 1 MHz for polycrystalline sample in the heating run.

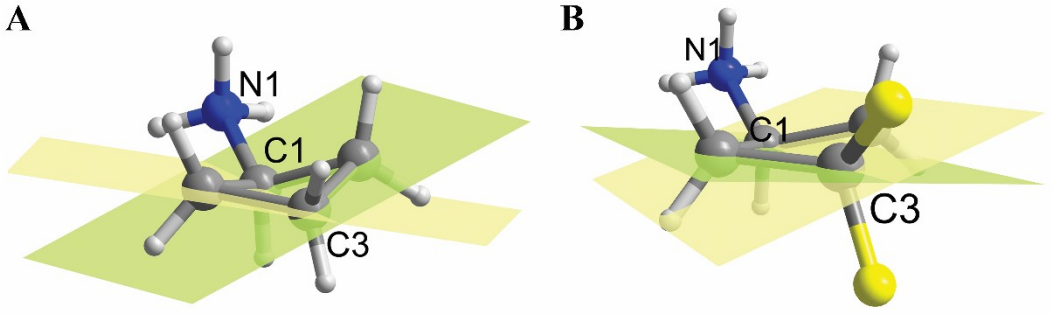

Fig. S5. Schematic diagram of the effect of F/H substitution on the molecular structure of CBA.

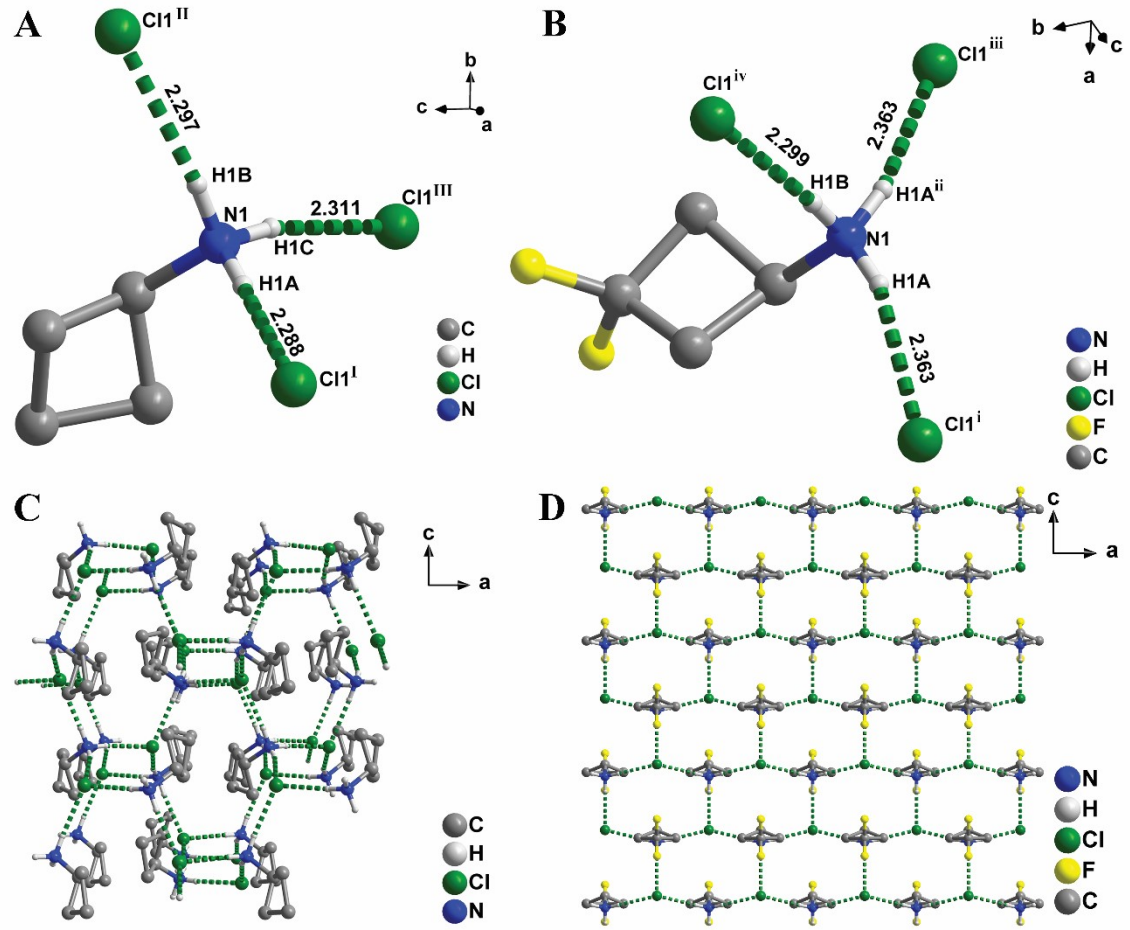

Fig. S6. The hydrogen bonding interactions profile of (CBA)Cl (A) and (3,3-DFCBA)Cl (B) in the LTP. And the packing views of (CBA)Cl (C) and (3,3-DFCBA)Cl (D) in the *ac* plane in the LTP. Hydrogen atoms bonded to C atoms were omitted for clarity.

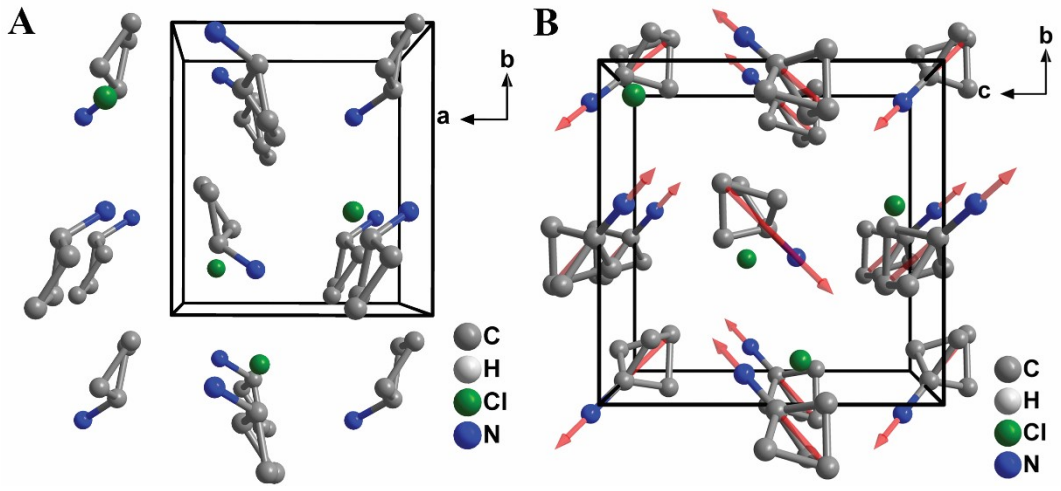

Fig. S7. The crystal structures of (CBA)Cl at 293 K (A) and 343 K (B), showing the similarities of crystal structures and the differences of orientation states of organic cations. The red arrow through CBA molecules represent the three-fold rotation axes. H atoms were omitted for clarity.

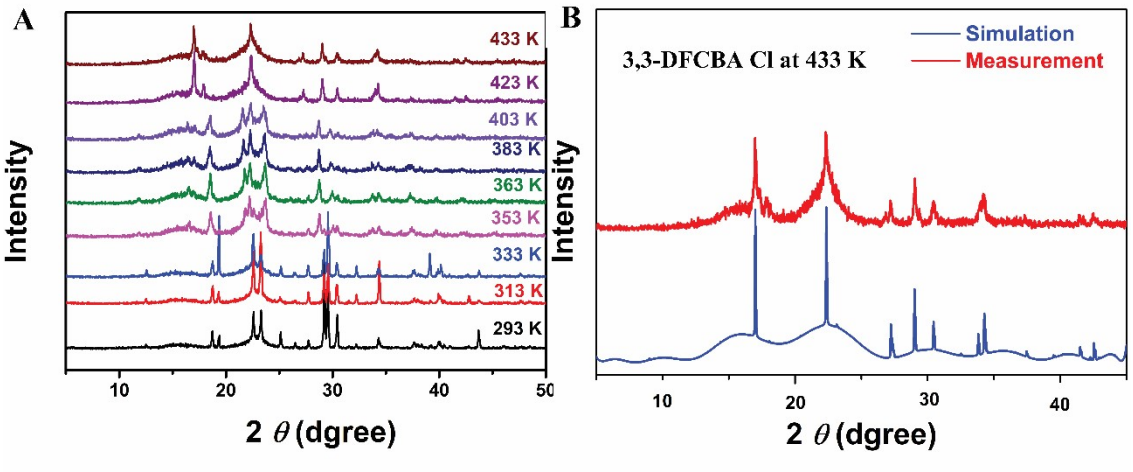

Fig. S8. The variable-temperature PXRD patterns of (3,3-DFCBA)Cl (A) and the pawley refinement of PXRD data of (3,3-DFCBA)Cl (B) at 433 K.

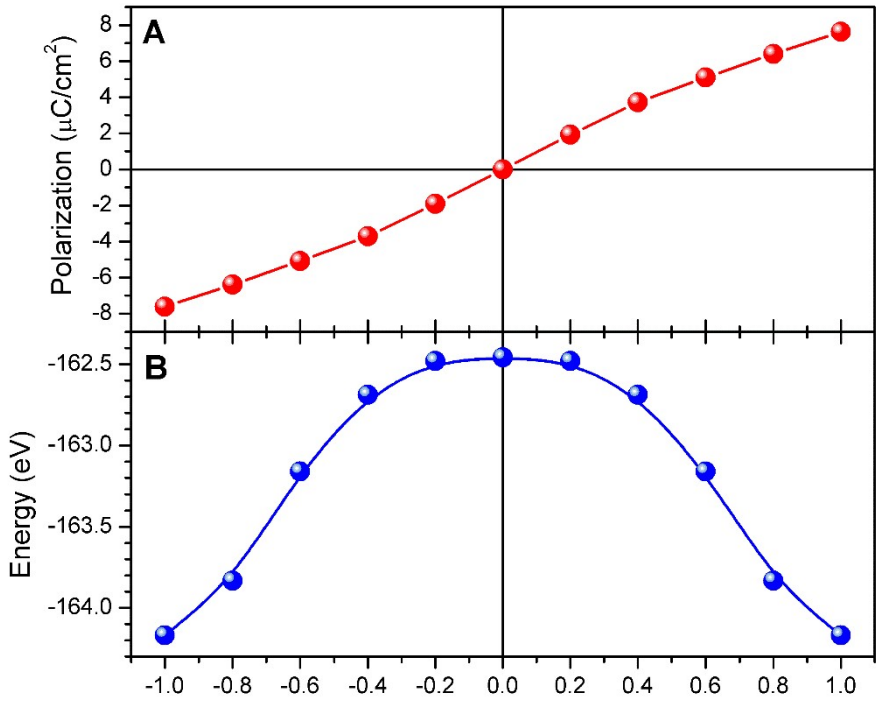

Fig. S9. Ferroelectric switching process of (3,3-DFCBA)Cl by DFT calculation. (A) Ferroelectric polarization evolution and (B) energy variation as a function of structure parameter λ.

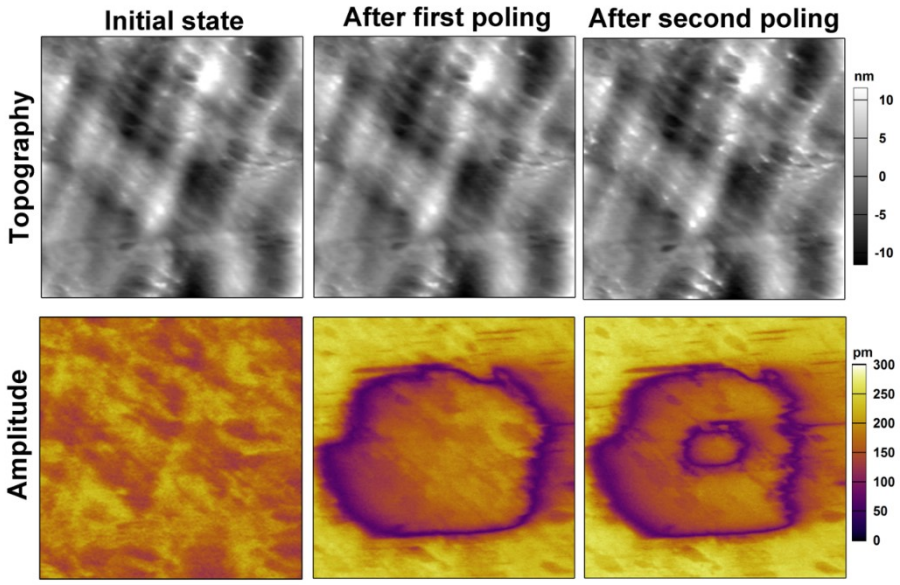

Fig. S10. Topography and vertical PFM amplitude images during the electric poling of the same region shown in Fig. 4G-I for the (3,3-DFCBA)Cl thin film.

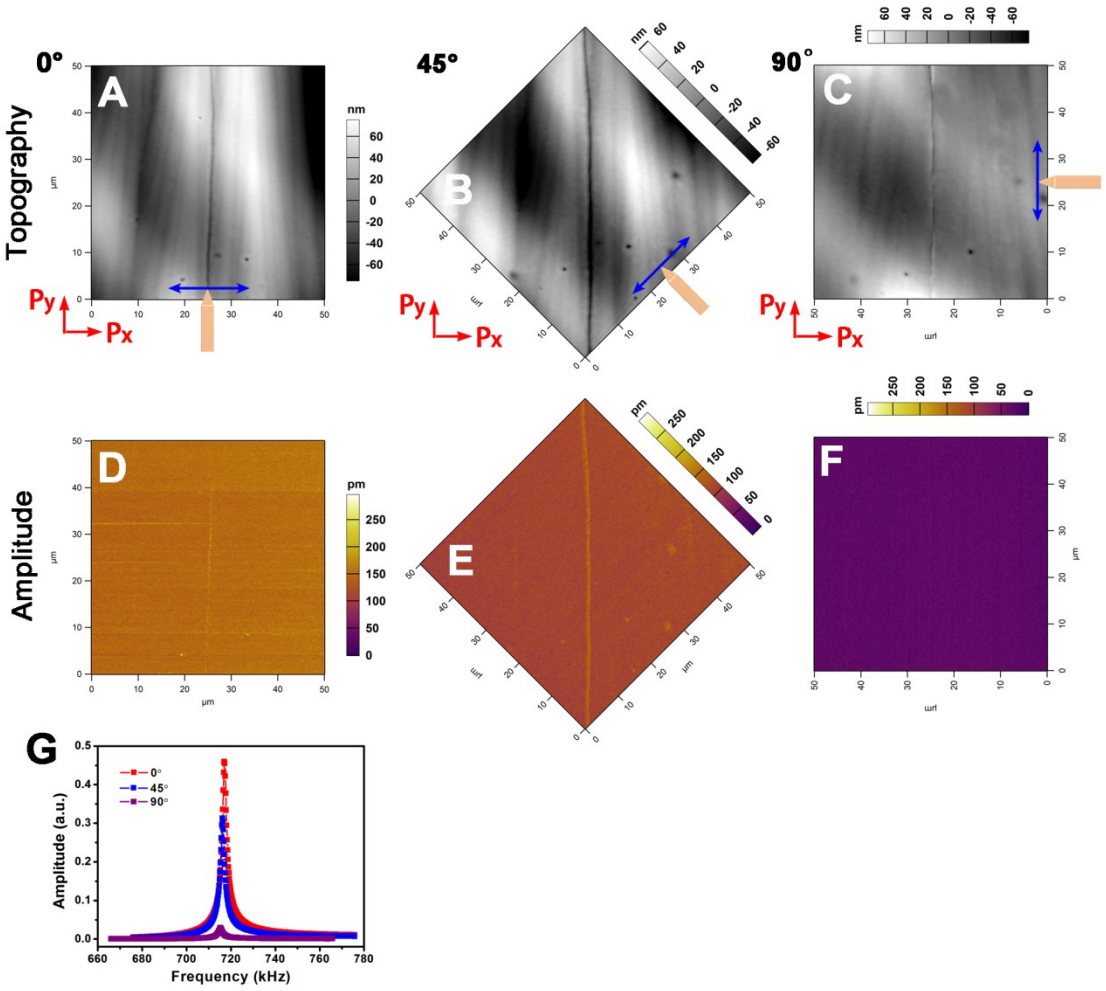

Fig. S11. PFM for (3,3-DFCBA)Cl thin film. (A-C) Topographic images around the selected region at rotation angles of 0°, 45° and 90°, respectively. (D-F) Corresponding lateral PFM amplitude images (drive voltage 2V). (G) Amplitude as a function of frequency for the film at rotation angles of 0°, 45° and 90° (drive voltage 2V). The insets in A, B and C are the PFM cantilever and the scanning direction.

With the probing ac field, the in-plane component of the polarization gives rise to local vibration in the lateral direction, which was monitored by PFM cantilever twisting or torsion (lateral PFM). The lateral PFM amplitude signal is proportional to $P_{//}\sin\theta$ (where $P_{//}$ is the in-plane polarization

component, θ is the alignment angle between the cantilever axis and $P_{//}$). We firstly performed angular-resolved PFM by rotating the sample with respect to the cantilever axis. We set the rotation angle is 0° where the lateral PFM of the film is strongest, and the measured in-plane polarization component was set as P_x (fig. S11A and D). Thus the piezoelectric response comes from piezoelectric coefficient d_{31}. Fig. S11E and F display the lateral PFM amplitude images at rotation angles of 45° and 90°, respectively. The amplitude represents a moderate signal at rotation angle of 45° and a weak signal at rotation angle of 90°. Fig. S11G shows the amplitude against the frequency for the film at rotation angles of 0°, 45° and 90° under drive voltage of 2 V. Again, the resonance shows a same relative magnitude.

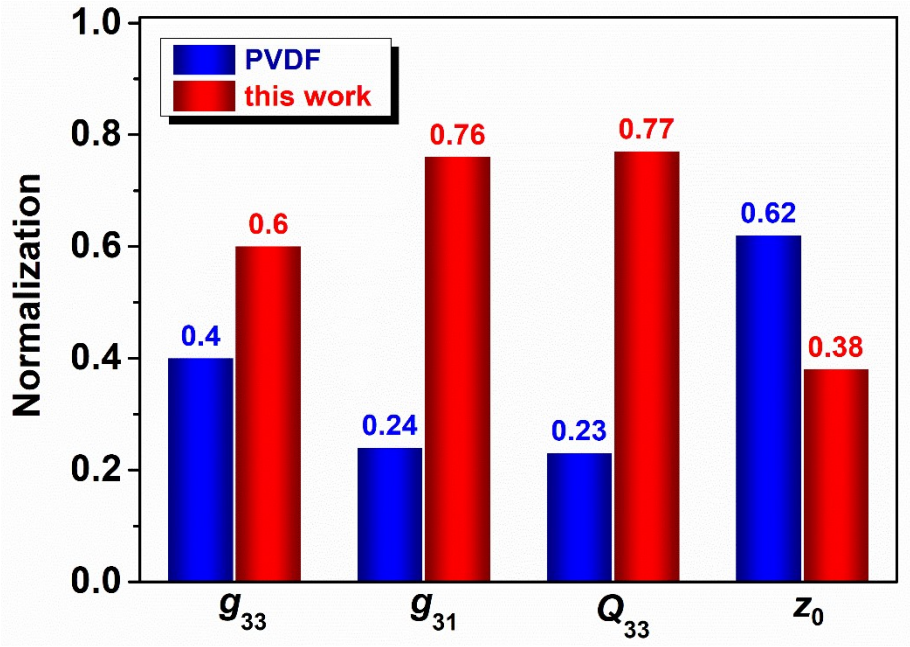

Fig. S12. Comparison of piezoelectric voltage coefficient g_{33}, g_{31} and Q_{33}, and acoustic impedance z_0 between ferroelectric polymer PVDF and (3,3-DFCBA)Cl thin films.

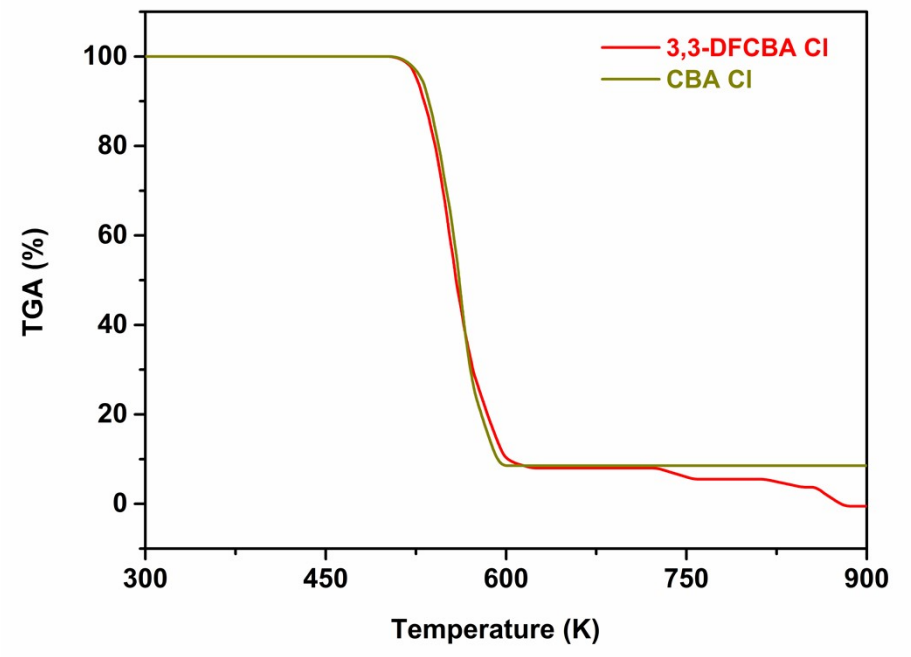

Fig. S13. Thermogravimetric analysis (TGA) curves of (3,3-DFCBA)Cl and (CBA)Cl, respectively.

Table S1. Comparison of (CBA)Cl and (3,3-DFCBA)Cl for various physical properties.

Compound	(CBA)Cl	(3,3-DFCBA)Cl
ε' (1 kHz)	2.6	7.88
T_c	318.6 K	374.4 K, 426 K
Aizu notation	23F222	4/*mmm*F*mm*2
Piezoelectric constant	d_{11}, d_{25}, d_{36}	d_{31}, d_{32}, d_{33}, d_{24}, d_{15}

Table S2. Crystal data and structure refinements for (CBA)Cl and (3,3-DFCBA)Cl at various temperatures.

Compound		(CBA)Cl	(3,3-DFCBA)Cl
Temperature	293 K	343 K	293 K
Formula	$C_4H_{10}NCl$	$C_4H_{10}NCl$	$C_4H_8F_2NCl$
Formula weight	107.58	107.58	143.56
Crystal system	orthorhombic	cubic	orthorhombic
Space group	$P2_12_12_1$	$P2_13$	$Pmn2_1$
a, *b*, *c* (Å)	7.8522(6) 8.8201(6) 8.9227(6)	8.5648(3) 8.5648(3) 8.5648(3)	6.0473(4) 7.0878(5) 7.6493(5)
α, β, γ (°)	90 90 90	90 90 90	90 90 90
Volume /Å^3	617.96(8)	628.28(7)	327.87(4)
Z	4	4	2
Density/g cm^{-3}	1.156	1.137	1.454
R_1	0.0512	0.0886	0.0348
wR_2	0.1521	0.3194	0.0851
GOF	1.071	1.076	1.073

Table S3. The contrast of molecular structure distortion for (CBA)Cl and (3,3-DFCBA)Cl.

Compound	(CBA)Cl	(3,3-DFCBA)Cl
plane angle (°)	32.677	22.664
<N1-C1-C3 (°)	146.049	139.567

Table S4. Hydrogen-bond geometry (Å, °) for (CBA)Cl and (3,3-DFCBA)Cl.

Compound	*D*—H···*A*	H···*A*	*D*···*A*	<*D*—H···*A*
(CBA)Cl	N1-H1A···Cl1^{I}	2.29 (2)	3.18 (2)	174.00 (2)
at 293 K	N1-H1B···Cl1^{II}	2.30 (2)	3.17 (2)	166.95 (2)
	N1-H1C···Cl1^{III}	2.31 (2)	3.18 (2)	167.11 (2)
(CBA)Cl	N1-H1A···Cl1$^{\alpha}$	2.37 (2)	3.17 (2)	146.87 (2)
at 343 K	N1-H1B···Cl1$^{\beta}$	2.38 (2)	3.17 (2)	146.69 (2)
	N1-H1C···Cl1$^{\gamma}$	2.37 (2)	3.17 (2)	146.64 (2)
(3,3-DFCBA)Cl	N1-H1A···Cl1^{i}	2.36 (1)	3.22 (1)	162.54 (2)
at 293 K	N1-H1A^{ii}···Cl1^{iii}	2.36 (1)	3.22 (1)	162.54 (2)
	N1-H1B···Cl1^{iv}	2.30 (1)	3.18 (1)	175.72 (2)

Symmetry codes: (I) x+1, y, z; (II) -x+1, y+1/2, -z+1/2; (III) x+1/2, -y+3/2, -z; (α) x+1/2, -y+3/2, -z; (β) x+1, y, z; (γ) -x+3/2, -y+1, z-1/2; (i) −x+1/2, −y+1, z−1/2; (ii) -x, y, z; (iii) –x-1/2, −y+1, z−1/2; (iv) x, y, z-1.

Table S5. Piezoelectric voltage coefficient of (3,3-DFCBA)Cl compared with some inorganic single crystals, textured ceramics, polymer, and molecular ferroelectrics including BTO, $0.99KNLN_{0.87}ST_{0.1}$-0.01CZ ceramic (KNN-ceramic), 0.71PMN-0.29Pt (PMNT29), $Pb(Mg_{1/3}Nb_{2/3})O_3$-$PbZrO_3$-$PbTiO_3$ (PMN-PZT), $(K_{0.5}Na_{0.5})$-$(Nb_{0.97}Sb_{0.03})O_3$ ceramics (Textured-KNNS), Sm and Mn-modified PT ceramic (SM-PT), triglycine sulfate (TGS), croconic acid (CA), diisopropylammonium bromide (DIPAB), PVDF, and so on. TPAP = triphenyl isopropylaminophosphonium, DPDP = diphenyl diisopropylaminophosphonium, TIAP = tetraisopropylaminophosphonium, FF = diphenylalanine, Dip = *β*,*β*-diphenyl-Ala-OH, Boc = tert-butyloxycarbonyl, 4,4′-Bpy = 4,4′-bipyridine, AcA = *N*-acetyl-L-alanine.

Samples	ε_r	d_{33} (pC N^{-1})	g_{33} (10^{-3} VmN^{-1})	Ref.
Textured-KNNS	382	208	61.5	(*54*)
KNN-basd ceramic	1027	275	30.26	(*11*)
Sm,Mn-doped $PbTiO_3$	196	59	34	(*55*)
$PbTiO_3$ single crystal	126	143	129	(*56*)
BTO ceramic	1892	191	11.4	(*57*)
BTO single crystal	168	85.6	57.6	(*57*)
PZT	730	220	34	(*58*)
PMNT29	5400	1500	31.37	(*59*)
PMN-PZT	4850	1530	35.63	(*59*)
SM-PT	124	127	115	(*60*)
PVDF	13	33	286.7	(*61*)
TGS	67	22	37.1	(*34*)
CA	12	5	47.1	(*34, 62*)
DIPAB	80	11	15.5	(*34, 29*)
$TPAP{\cdot}BF_4$	9.28	3	36.5	(*48*)
$TPAP{\cdot}ClO_4$	16.21	4	27.87	(*48*)
$DPDP{\cdot}BF_4$	7.26	7	108.9	(*48*)
$DPDP{\cdot}ClO_4$	9.08	12	149.3	(*48*)
$DPDP{\cdot}IO_4$	8.75	8	103.3	(*48*)
$TIAP{\cdot}BF_4$	16.67	3	20.3	(*48*)
$TIAP{\cdot}ClO_4$	16.88	3	20.1	(*48*)
Boc-Dip-Dip	3−4	73.1 ± 13.1	2000-3000	(*49*)
Boc-FF	−	8.4 ± 1.7	−	(*49*)
FF	−	18	−	(*49*)
4,4′-Bpy	3.13	20.9	1150	(*50*)
AcA	2.24	9.5	480	(*50*)
4,4′-Bpy/AcA	2.51	14.9	670	(*50*)
$DPDP{\cdot}PF_6$	−	8	−	(*53*)
(3,3-DFCBA)Cl	**7.88**	**30.5**	**437.2**	**This work**

Table S6. The value of acoustic impedance z_0 measured on different ferroelectric samples.

Ferroelectrics	ρ 10^3 kg m^{-3}	c 10^3 m s^{-1}	Measured z_0 10^6 kg s^{-1} m^{-2}	Reference z_0 10^6 kg s^{-1} m^{-2}	Source
PZT ($Pb(Zr_{0.52}Ti_{0.48})O_3$)	7.50	3.39	25.39	30 (*63*)	Purchased from Hefei Ke Jing Materials Technology Co., Ltd. http://www.kjmti.com/
BTO	5.30	3.97	21.05	22.0-32.7 (*64*)	Purchased from Hefei Ke Jing Materials Technology Co., Ltd. http://www.kjmti.com/
LNO ($LiNbO_3$)	4.34	10.06	43.64	19.55 (*64*)	Purchased from Hefei Ke Jing Materials Technology Co., Ltd. http://www.kjmti.com/
Rochelle salt	1.79	4.21	7.54	5.49 (*64*)	Prepared by ourselves according to the literature (*65*)
PVDF	1.78	2.39	4.25	3.92 (*64*), 3.9 (*66*)	Purchased from MEAS, USA http://www.te.com/usa-en/products/families/meas.html
PVDF	1.63	2.26	3.69		Prepared by ourselves by hot press molding
TGS	1.69	5.76	9.74		Prepared by ourselves according to the literature (*67*)
DIPAB	1.34	3.27	4.39		Prepared by ourselves according to the literature (*29*)
(3,3-DFCBA)Cl	**1.19~1.45**	**1.55~2.55**	**2.25~3.26**		**This work**

Acoustic impedance and specific acoustic impedance are measures of the opposition that a system presents to the acoustic flow resulting from an acoustic pressure applied to the system. Specific acoustic impedance z is an intensive property of a particular material. The absolute value of this specific acoustic impedance is often called "characteristic specific acoustic impedance" and denoted z_0:

$$z_0 = \rho c$$

where ρ is the volumetric mass density of the material, c is the speed of the sound waves traveling in the material.

All measurements were done in our lab using Ultrasonic Sound Velocity Testing Device (CGN Inspection Technology Co., Ltd. China) via "Density-Speed" method described above. All samples were immersed in silicone oil as medium at room temperature during the measurements.

Dielectric permittivity and piezoelectric coefficient matrix

Considering the point group $mm2$ of (3,3-DFCBA)Cl in its ferroelectric phase, the dielectric constant matrix $[\varepsilon]$ can be written as:

$$\begin{bmatrix} \varepsilon_{11} & 0 & 0 \\ 0 & \varepsilon_{22} & 0 \\ 0 & 0 & \varepsilon_{33} \end{bmatrix}$$

the piezoelectric constant matrix $[d]$ can be written as:

$$\begin{bmatrix} 0 & 0 & 0 & 0 & d_{15} & 0 \\ 0 & 0 & 0 & d_{24} & 0 & 0 \\ d_{31} & d_{32} & d_{33} & 0 & 0 & 0 \end{bmatrix}$$

The element d_{33} is the longitudinal piezoelectric coefficient, which characterizes the volume change as response to an applied electric field in the same direction.

Considering the point group 222 of ((CBA)Cl) in its room-temperature phase, the piezoelectric constant matrix $[d]$ can be written as:

$$\begin{bmatrix} 0 & 0 & 0 & d_{14} & 0 & 0 \\ 0 & 0 & 0 & 0 & d_{25} & 0 \\ 0 & 0 & 0 & 0 & 0 & d_{36} \end{bmatrix}$$

Reference:

49. R. King-Smith and D. Vanderbilt, *Phys. Rev. B*, 1993, **47**, 1651.
50. D. Vanderbilt and R. King-Smith, *Phys. Rev. B*, 1993, **48**, 4442.
51. G. Kresse and J. Furthmüller, *Phys. rev. B*, 1996, **54**, 11169.
52. G. Kresse and J. Furthmüller, *Comput. Mater. Sci.*, 1996, **6**, 15-50.
53. J. P. Perdew, K. Burke and M. Ernzerhof, *Phys. rev. lett.*, 1996, **77**, 3865.
54. Y. Chang, S. F. Poterala, Z. Yang, S. Trolier-McKinstry, G. L. Messing, *Appl. Phys. Lett.*, 2009, **95**, 232905.
55. S. Ikegami, I. Ueda, T. Nagata, *J. Acoust. Soc. Am.*, 1971, **50**, 1060-1066.
56. T. Suwannasiri, A. Safari, *J. Am. Ceram. Soc.*, 1993, **76**, 3155-3158.
57. R. E. Newnham, L. J. Bowen, K. A. Klicker, L. E. *Cross, Mater. Des.*, 1980, **2**, 93-106.
58. C. A. Randall, N. Kim, J.-P. Kucera, W. Cao, T. R. Shrout, *J. Am. Ceram. Soc.*, 1998, **81**, 677-688.
59. S. Zhang, S.-M. Lee, D.-H. Kim, H.-Y. Lee, T. R. Shrout, *J. Appl. Phys.*, 2007, **102**, 114103.
60. Y. Yan, J. E. Zhou, D. Maurya, Y. U. Wang, S. Priya, *Nat. Commun.*, 2016, **7**, 13089.
61. M. Li, H. J. Wondergem, M.-J. Spijkman, K. Asadi, I. Katsouras, P. W. M. Blom, D. M. de Leeuw, *Nat. Mater.*, 2013, **12**, 433-438.
62. S. Horiuchi, Y. Tokunaga, G. Giovannetti, S. Picozzi, H. Itoh, R. Shimano, R. Kumai, Y. Tokura, *Nature*, 2010, **463**, 789-792.
63. P. P. L. Regtien, Sensors for Mechatronics. (Elsevier, 2012).
64. Y. Li, Z.-K Qin, Z.-Y Zhou, Measurement of piezoelectric and ferroelectric materials. (Science Press, Beijing, 1984).
65. J. Curie, P. Curie, C. R. *Acad. Sci. Paris*, 91, 294-297 (1880).
66. F. S. Foster, K. A. Harasiewicz, M. D. Sherar, *IEEE Trans. Ultrason., Ferroelect., Freq. Contr.*, 2000, **47**, 1363-1371.
67. S. Hoshino, T. Mitsui, F. Jona, R. Pepinsky, *Phys. Rev.*, 1957, **107**, 1255.